RSC Advances

ROYAL SOCIETY OF CHEMISTRY

www.rsc.org/advances

Aluminum-doped Zinc Oxide nanoparticles with tunable near-infrared absorption/reflectance by a simple solvothermal process

Haifeng Zhou, Hua Wang, Kang Zheng, Zhen Gu，Zhaofeng Wu, Xingyou Tian*

Key Laboratory of Materials Physics, Institute of Solid State Physics, Chinese Academy of Sciences, Hefei 230031, China

*Corresponding author: xytian@issp.ac.cn, Phone: (+86) 5515591477, Fax: (+86)5515591434.

Abstract

Transparent conductive oxides have attracted wide attention over past decade due to the great potential applications. In this manuscript, we report the preparation of the aluminum-doped zinc oxide (AZO) nanoparticles (NPs) through the solvothermal method. The effective incorporation of Al as a dopant is demonstrated by tracking free carrier absorption in the infrared region and energy-dispersive X-ray spectroscopy (EDX). The obtained AZO NPs present tunable absorption and reflectance in the near infrared (NIR) range at different doping levels. Moreover, the optimal precursor ration of Al to (Al+Zn) is 4mol% to receive the largest NIR reflectance and absorbance of AZO NPs.

Key words

near-infrared absorption, Zinc Oxide, doping.

1. Introduction

Transparent conductive oxides (TCOs) are considered as a technologically important class of materials because of their unique combination of good electrical

conductivity, high chemical stability, visible light transparency and near infrared light reflectance/absorption.[1-9] For example, TCOs such as antimony-doped tin oxide (ATO),[10] tin-doped indium oxide (ITO),[4] fluorine-doped tin oxide (FTO),[11] aluminum-doped zinc oxide (AZO),[12] gallium-doped zinc oxide (GZO),[13] and indium-doped zinc oxide (IZO) play a critical role in photovoltaic cells, [2,14] energy-efficient windows, flat panel displays, light emitting diodes (LED) and liquid crystal display (LCD). Among them, ZnO based materials have recently gained more and more interests owing to both the low price and nontoxicity.[15-18] Thus, they have been thought to be a promising alternative to indium based TCOs because of indium's rarity and thus high price.

ZnO is one of the most important wide-band-gap materials that have superior electronic and optical properties. In order to enhance its performance in view of electronic and optical properties doping is essential.[13,19-24] Synthetic control over doping of ZnO NPs has made dramatic strides and a great number of strategies such as co-precipitation method, microwave heating route，wet chemical route can now be used to prepare ZnO NPs with good control over size and physical properties. By introducing the high-valence elements (group III elements Al, Ga, or In) into ZnO crystals, the oxide becomes nonstoichiometric, and the success of doping is often accompanied by changes in optical and electrical properties of ZnO nanostructures. It should be noted that only effective doping incorporation within the crystalline lattice would lead to the desired electrical and optical properties. Effective doping incorporation means that dopants occupy substitutional sites in the interior of the

particles rather than just being adsorbed on the nanocrystal surface.[25-27] The vast majority of investigations of ZnO doping have been conducted to prepare doped ZnO with desired morphology and size, and these researches mainly focused on enhancement of the electrical properties. However, there are only few reports on the optical properties of doped ZnO. Delia J. Milliron [22] prepared AZO nanocrystals colloidal with tunable infrared absorption and visible transparency through hot injection method. Alessandro Martucci [13] used the same routine to synthesis GZO colloidal with optical and electrical performances directly comparable with ITO colloidal coatings.

In this manuscript, we report the preparation the AZO NPs using the solvothermal method. The morphology and entire growth process of AZO NPs were studied by XRD and TEM. The effective incorporation of Al as a dopant is demonstrated by tracking free carrier absorption in the infrared region and energy-dispersive X-ray spectroscopy (EDX).The near-infrared absorption/reflectance of AZO NPs were investigated by UV–VIS–NIR spectrophotometer.

2. Experimental Section

2.1 Raw materials

$Al(NO_3)_3 \cdot 9H_2O$, $Zn(CH_3COO)_2 \cdot 2H_2O$ and ethanol were purchased from Qiang Shen Chemical Reagent Co., Ltd. Nanjing, China.

2.2 Preparation of AZO NPs

AZO NPs were prepared by solvothermal method similar to that described in previous work.[21] In a typical synthesis, a precursor solution containing mixture of

0.5mmol $Al(NO_3)_3 \cdot 9H_2O$ and 10 mmol $Zn(CH_3COO)_2 \cdot 2H_2O$ in a 40 mL ethanol were added into a 50 mL Teflon lined stainless steel autoclave. Subsequently, the autoclave was kept at 140 ºC for 6 h. After cooling down to room temperature, the resulting precipitate is centrifuged and washed thoroughly with water and methanol several times. The precipitate is finally dried in a furnace at 60 ºC in air and the amount of the obtained AZO NPs was about 1.6g. The prepared AZO NPs were dispersed in ethanol and deposited on glass substrates by spin coating to obtain AZO thin films. By changing the content of the $Al(NO_3)_3 \cdot 9H_2O$, different doping proportion of AZO NPs was prepared and coded as AZO-x, where x =Al/(Zn +Al)(Molar ratio).

2.3 Characterization

XRD patterns were carried out with a Philips X'pert-PRO using Cu-Ka radiation. The diffraction angle 2θ ranged from 10 to 90°. Fourier transform infrared (FTIR) spectroscopy was performed on a spectrometer (Nexus, Nicolet) using the attenuated total reflectance (ATR) technique. Data were collected at 4 cm^{-1} resolution co-adding 32 scans per spectrum. TEM and Energy Dispersive X-ray (EDX) analysis were obtained with a transmission electron microscope (JEM-2010). Thermogravimeter (Pyris 1 TGA) was used to measure the weight loss of the nanopaticles under N_2 atmosphere. The samples were heated from 100 ºC to 700 ºC at a heating rate of 10 ºC /min. Absorption spectra of the NPs dispersed in toluene, used for the band gap extrapolation, were recorded in the 250-800 nm spectral range. Optical absorption and reflectivity of the AZO thin films were measured with a UV3600 (Shimadzu, Japan)

UV–VIS–NIR spectrophotometer.

3. Results and discussion

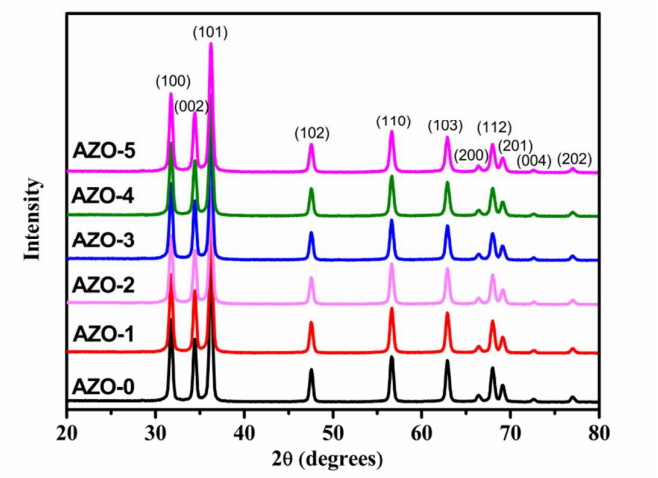

Fig. 1 XRD patterns of pure ZnO and AZO powders.

The structural implications of dopant incorporation in the AZO NPs were investigated by X-ray diffraction (XRD) (Fig.1). At all doping levels, the samples exhibited only pure wurtzite ZnO diffraction peaks (hexagonal phase, space group: P63/mc, JCPDS File Card No. 36-1451).[13] No other crystalline phases such as aluminum oxide (Al_2O_3) or gahnite ($ZnAl_2O_4$) which are common secondary phases in AZO thin films, can be observed. Furthermore, no significant variation in XRD peaks compared to the standard wurtzite pattern among the different samples in this study, but a slight variation in their relative intensity and broadening can be observed which are assigned to variations in the shape and size of the nanocrystals due to the presence of dopant ions.

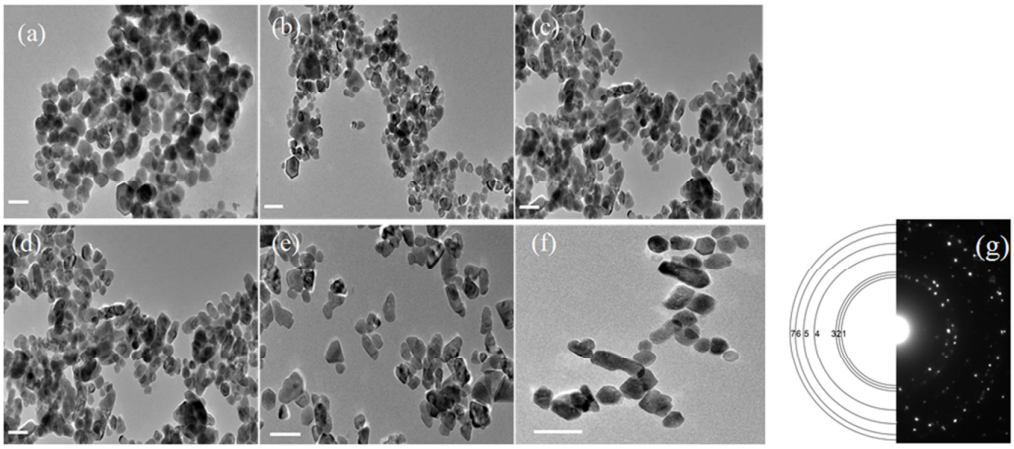

Fig. 2 TEM images of AZO NPs with different aluminum concentrations (a) 0%; (b) 1%; (c) 2%; (d) 3%; (e) 4% and (f) 5%. (Scale bars =100 nm). The image of (g) is the corresponding selected-area electron diffraction pattern of (f), the indexes of the diffraction rings are as follows: (1) (100), (2) (002), (3) (101), (4) (102), (5) (110), (6) (103), and (7) (200).

Transmission electron microscopy (Fig.2) investigations give further insight into the size and shape of AZO NPs with different doping levels. It is apparent that as for low Al concentration the AZO NPs show near-spherical NPs, while bigger NPs and more anisotropic shapes are obtained at higher Al concentration and the size distribution become broad as more Al doped. Thus, the incorporation of Al in the ZnO crystals has a strong impact on the shape and size of the NPs. The selected-area electron-diffraction pattern of AZO NPs clearly indicates the polycrystalline nature (Fig.2 (g)).

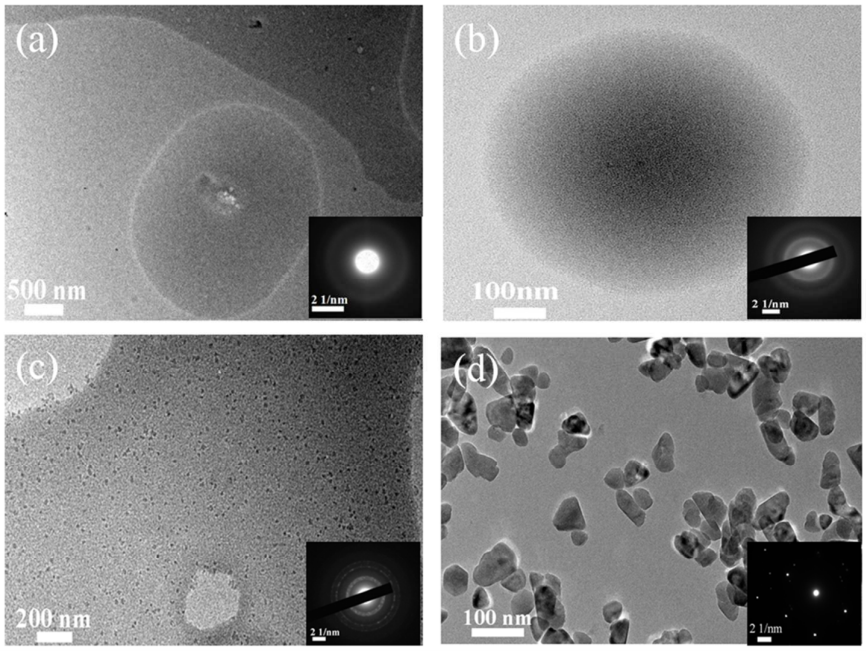

Fig.3 TEM images of AZON-4 for (a) 10 min; (b) 1 h; (c) 3 h and (d) 6 h, respectively.

In order to illuminate the mechanism of particle formation of AZO NPs, we investigated the morphology evolution of AZO-4 at different reaction times by TEM. It can be seen that gel emerged as the Fig. 3(a) shows. The inset of Fig. 3(a) confirms the amorphous nature of the gel. As reaction time proceed, some tiny crystallites emerged and embedded into the amorphous gel evidenced by the Fig. 3(b) which shows some tiny black dots randomly distributed in the gel and diameters are in the 5 nm range. The tiny crystallites underwent further crystal growth and the diameters increased to 20 nm approximately. And the SAED indicated a certain degree of crystallinity of the system, though the majority of its still kept strong amorphous phase (Fig. 3(c)). Accompanied by the disappearance of the gel, the growth of AZO NPs completed when the reaction period was proceeded for 6 h (Fig. 3(d)). Together with the abovementioned growth processes of four different periods in our case, we

can infer that the mechanism of particle formation involves three steps, condensation, nucleation and growth. In the first step, condensation reactions between metal carboxylates and alcohols give rise to the formation of the metal-oxygen-metal bond through the ester elimination process and metal oxide gel formed, and the main reactions in this given system can be summarized in Scheme 1. [9] Then, the nuclei and tiny crystallite emerged. Finally, they experienced further growth until the precursors are consumed in the solution.

$$Zn(CH_3COO)_2 + CH_3CH_2OH \longrightarrow \text{-Zn-OH} + CH_3COOCH_2CH_3$$

$$\text{-Zn-OH} + \text{-Zn-OH} \longrightarrow (ZnO)n + H_2O$$

Scheme 1. Condensation reaction between metal carboxylate and alcohol.

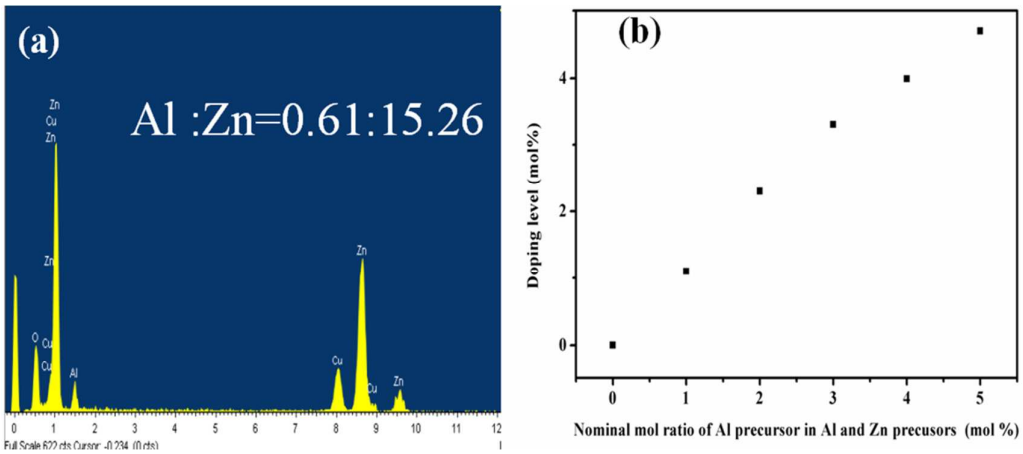

Fig. 4 (a) EDX spectra of AZO-4 and (b) doping level determined by EDX.

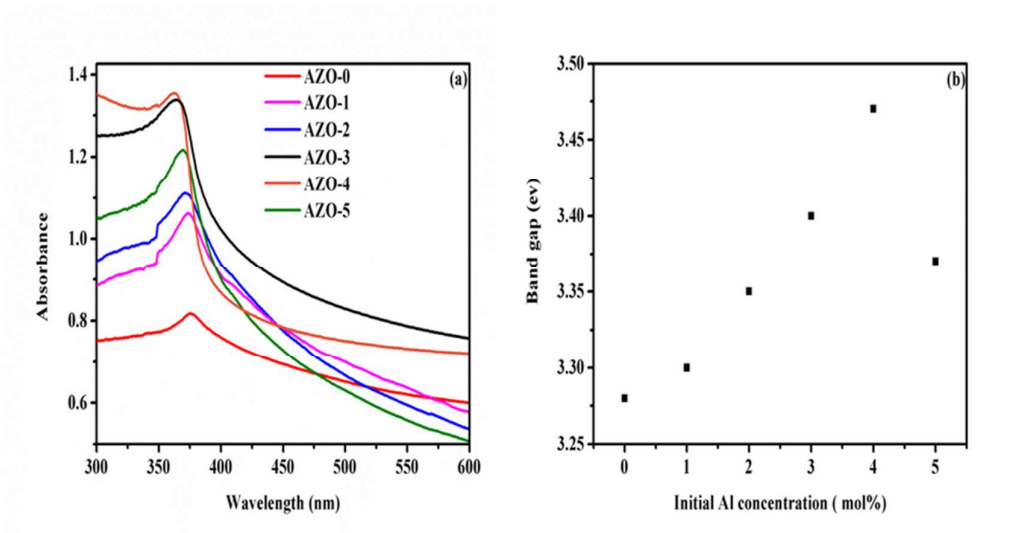

Fig.5 (a) Absorption spectra of the AZO NPs dispersed in toluene and (b) calculated band gap versus different initial Al concentrations.

To probe the chemical composition and the relative amount between Al and Zn, the AZO NPs was studied by elemental analysis with energy-dispersive X-ray spectroscopy (EDX). Fig. 4(a) shows that the EDS spectra of AZO-4 NPs are composed of the elements of C, O, Al, Cu, and Zn. The atomic ratio of Al and Zn is 0.21:15.26. Fig. 4(b) shows results of different doping level determined by EDX. It can be observed that ratios of Al estimated with EDX are larger than the initial input ratios of $Al(NO_3)_3 \cdot 9H_2O$ precursors. Though, the EDX can not accurately determine the value because of the limitation of the EDX measurement which provide local information including the dopants substituted into the NC core and that adsorbed on the NC surface, a clear change trend that the doping level increases as the ration of precursors increasing can be demonstrated. It is well known that the substitution of Al^{3+} (0.53 Å) for Zn^{2+} (0.74 Å) in the ZnO wurtzite structure can release electrons to the conduction band resulting in generation of free carriers and consequently cause an

increase of optical band gap due to Burnstein-Moss effect. [22,28]Thus, to further confirm the effective doping of Al in the ZnO NPs, the UV-VIS absorption spectra of the AZO NPs dispersed in toluene were investigated (Fig. 5(a)) and the band gap derived from plots of $(\alpha h\nu)^2$ versus the photon energy ($h\nu$) (extrapolating of the linear part of the absorption edge leads to the axis interception) are shown in Fig. 5(b). Increase of the optical band gap can be observed as the initial Al mol ratio increasing from the ratio of 0 mol% to 4 mol%. The blue shift of band gap provides further evidence of Al doping. However, in the case of AZO-5 the band gap is 3.36 ev which is lower than that of 3.48 ev of AZO-4 and 3.41 ev of AZO-3. It confirms that there exists a solubility limit of Al in ZnO lattice, beyond which the excess Al^{+3} do not occupy the proper substitutional lattice sites to increase free electrons, but rather go to interstitial sites, causing a decrease of free electron.[26] Therefore, we conclude that the ratio of $Al(NO_3)_3 \cdot 9H_2O$ precursor that can obtain the most effective doping in our experiment is 4 mol%, increasing the $Al(NO_3)_3 \cdot 9H_2O$ in the solution would cause a decrease of free electron.

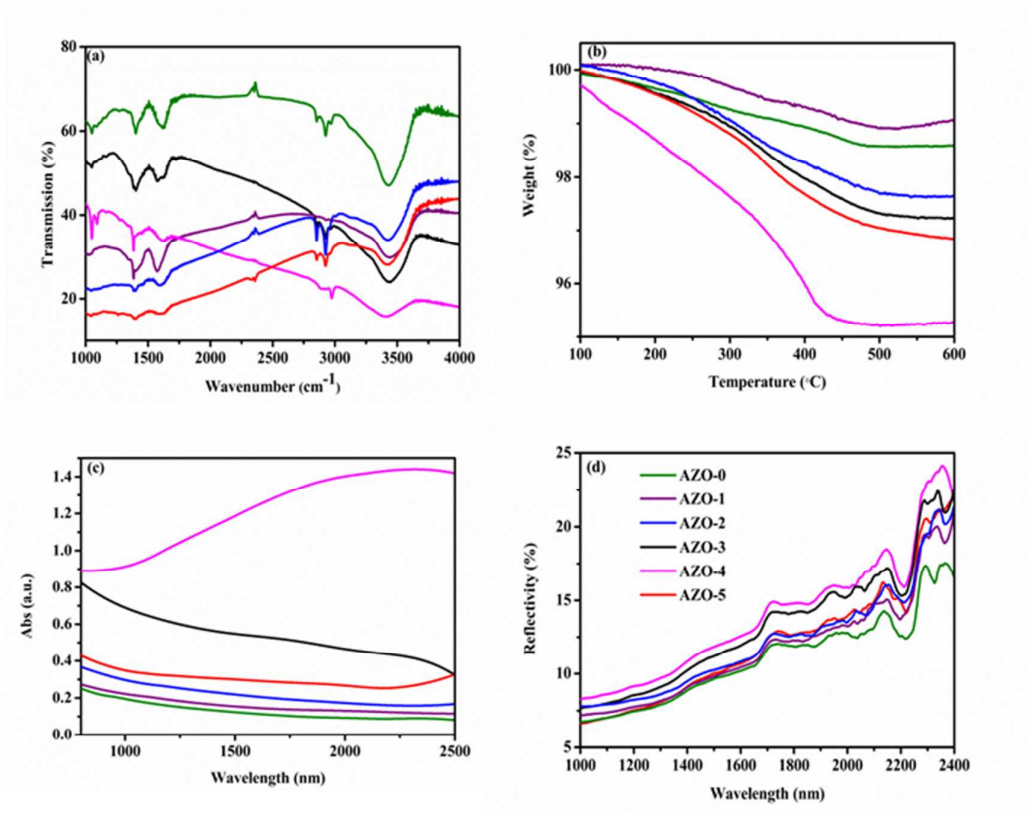

Fig. 6 FTIR spectra (a) and TGA curves (b) of AZO NPs. The optical absorbance (c) and reflectivity spectra (d) of AZO films as deposited by spin coating.

FT-IR measurements were performed and are shown in Fig. 6(a). Absorption peaks around 3420 cm^{-1}, 2976 cm^{-1}, 2928 cm^{-1}, 1638 cm^{-1}, 1405 cm^{-1} and 1044 cm^{-1} indicate some organic molecular and water adsorbed on the surface of AZO NPs. The mass fraction of these impurities deduced form the TGA curves (Fig. 6 (b)) are in the range from 0.8 wt% to 4.8 wt%. Furthermore, the absorption peak of AZO NPs increased in intensity and shifted to higher energies as the dopant concentration increased, except for the AZO-5 which exhibits a weaker absorption than AZO-4 and AZO-3. This result is consistent with observations evidenced by band gap calculation. It is well known that the replacement of Zn^{2+} ions by Al^{3+} would generate a plasmonic

resonance absorption in the infrared region and the absorption in the NIR is the onset of the plasmon resonance arising from the free carriers.[27,29,30] According to the Drude theory,[31] there is a free carrier plasma resonance frequency in the TCOs, the plasma resonance frequency can be expressed as the equation 1 below

$$\omega_\rho = \sqrt{\frac{ne^2}{\varepsilon_0 \varepsilon_\infty m_c^*}}$$

where n is the carrier concentration, e is the electronic charge, ε_0 is the permittivity of free space, ε_∞ is the high- frequency permittivity, and m_c is the conductivity effective mass in the amount of free carriers. Apparently, the plasmon resonance frequency is proportional to the square root of the free electron concentration. Inferring form the calculations of band gap and results of FT-IR measurements we could confirm that the carrier concentration initially increases form AZO-1 to AZO-4 NPs and then decreases as to the AZO-5 NPs. Thus, the increasing of free carriers lead to the enhancement absorption of AZO thin films form AZO-1 to AZO-4 NPs, while the AZO-5 thin film present a weaker absorption than the AZO-4 and AZO-3 films, as shown in Fig. 6(c). Apparently, the AZO-4 exhibits the most strong plasmon resonance absorption and the peak deduced from Fig. 6(c) is about 2400 nm. Thus, we conclude that the range of the plasma resonance frequency is lower than 1.9 ev under our experiments. Fig. 6(d) shows the reflectivity spectra of AZO films which are in good accordance with the changing trend of plasmon resonance absorption and the AZO-4 exhibits the strongest reflection. This is because of that when the frequency of the light is lower than the frequency of the plasma resonance frequency in the material, the light will be reflected. Thus, the reflectivity initially underwent a gradual

enhancement due to the increasement of plasma resonance frequency.

Conclusions

In this work, AZO NPs were prepared through the solvothermal method. The XRD results indicated that the samples exhibited only pure wurtzite ZnO diffraction peaks at doping levels. The mechanism of particle formation involves three steps, condensation, nucleation and growth. At high doping level, the morphology of AZO NPs became slightly anisotropic. From the bandgap analysis, we conclude that the ratio of $Al(NO_3)_3 \cdot 9H_2O$ precursor that can obtain the most effective doping in our experiment is 4 mol%, increasing the $Al(NO_3)_3 \cdot 9H_2O$ in the solution would cause a decrease of free electron. The obtained AZO-4 NPs presented the largest absorption and reflectance in NIR range.

Acknowledgements

The authors are grateful to the support of National Natural Science Foundation of China (No. 51103160) and Youth Exchange Promotion Association.

References

1 R. M. Pasquarelli, D. S. Ginley and R. O'Hayre, *Chem. Soc. Rev*， 2011,**40**,5406.
2 M. A. Lucio-Lopez, M. A. Luna-Arias, A. Maldonado, M. D. Olvera and D. R. Acosta, *Sol. Ener. Mat. Sol. C*. 2006, **90**, 733.
3 K. Zilberberg, J. Meyer and T. Riedl, *J. Mater.Chem. C*, 2013, **1**, 4796.
4 M. Kanehara, H. Koike, T. Yoshinaga and T. Teranishi, *J.AM.Chem.Soc*, 2009, **131**, 17736.
5 L. Luo, M. D. Rossell, D. Xie, R. Erni and M. Niederberger, *Acs. Sus.Chem. Eng*, 2013, **1**, 152.
6 E. Redel, C. Huai, O. Dag, S. Petrov, P. G. O'Brien, M. G. Helander, J. Mlynarski and G. A. Ozin, *Small*,2012, **8**, 3806.
7 D. Ebert and B. Bhushan, *Langmuir*, 2012, **28**, 11391.
8 M. Epifani, R. Diaz, J. Arbiol, E. Comini, N. Sergent, T. Pagnier, P. Siciliano, G. Faglia and J. R. Morante, *Adv. Funct.Mater*, 2006, **16**, 1488.
9 N. Pinna and M. Niederberger, *Angew. Chem.Int.Edit*., 2008, **47**, 5292.

10 Y. Wang, T. Brezesinski, M. Antonietti and B. Smarsly, *Acs.Nano*, 2009, **3**, 1373.
11 B. Zhang, Y. Tian, J. X. Zhang and W. Cai, *Appl.Phys.lett*, 2011, **98**.
12 Y.-S. Luo, J.-P. Yang, X.-J. Dai, Y. Yang and S.-Y. Fu, *J. Phys. Chem. C*, 2009, **113**, 9406.
13 E. Della Gaspera, M. Bersani, M. Cittadini, M. Guglielmi, D. Pagani, R. Noriega, S. Mehra, A. Salleo and A. Martucci, *J.AM.Chem.Soc*, 2013, **135**, 3439.
14 S. Sanctis, R. C. Hoffmann and J. J. Schneider, *Rsc. Adv*, 2013, **3**, 20071.
15 B. Wen, Y. Huang and J. J. Boland, *J. Phys. Chem. C,* 2008, **112**, 106.
16 Y. Q. Li, S. Y. Fu and Y. W. Mai, *Polymer*, 2006, **47**, 2127.
17 M. L. Kahn, M. Monge, V. Colliere, F. Senocq, A. Maisonnat and B. Chaudret, A*dv. Funct.Mater*, 2005, **15**, 458.
18 H. Wang, L. Jia, P. Bogdanoff, S. Fiechter, H. Moehwald and D. Shchukin, *Energ. Environ. Sci*,2013, **6**, 799.
19 X. H. Huang, C. Zhang, C. B. Tay, T. Venkatesan and S. J. Chua, *Appl.Phys.lett*, 2013,**102**, 111106.
20 X. H. Huang, Z. Y. Zhan, K. P. Pramoda, C. Zhang, L. X. Zheng and S. J. Chua, *Crystengcomm*, 2012, **14** , 5163.
21 Z. Lu, J. Zhou, A. Wang, N. Wang and X. Yang, *J. Mater.Chem*., 2011, **21**, 4161.
22 R. Buonsanti, A. Llordes, S. Aloni, B. A. Helms and D. J. Milliron, *Nano. Lett,* 2011, **11**, 4706.
23 M. P. Taylor, D. W. Readey, M. F. A. M. van Hest, C. W. Teplin, J. L. Alleman, M. S. Dabney, L. M. Gedvilas, B. M. Keyes, B. To, J. D. Perkins and D. S. Ginley, *Adv. Funct.Mater*, 2008, **18**, 3169.
24 R. P. Wang, A. W. Sleight and D. Cleary, *Chem. Mater*, 1996, **8**, 433.
25 R. Buonsanti and D. J. Milliron, *Chem. Mater*, 2013, **25**, 1305.
26 A. Kelchtermans, K. Elen, K. Schellens, B. Conings, H. Damm, H.-G. Boyen, J. D'Haen, P. Adriaensens, A. Hardy and M. K. Van Bael, *Rsc. Adv*, 2013, **3**, 15254.
27 D. J. Norris, A. L. Efros and S. C. Erwin, *Science*, 2008, **319**, 1776.
28 J.-Y. Oh, S.-C. Lim, S. D. Ahn, S. S. Lee, K.-I. Cho, J. B. Koo, R. Choi and M. Hasan, *J.Phys.D.Appl.Phys*., 2013, **46**.
29 D. J. Rowe, J. S. Jeong, K. A. Mkhoyan and U. R. Kortshagen, *Nano.Lett*, 2013, **13**, 1317.
30 L. De Trizio, R. Buonsanti, A. M. Schimpf, A. Llordes, D. R. Gamelin, R. Simonutti and D. J. Milliron, *Chem.Mater*, 2013, **25**, 3383.
31. M. Kojima, H. Kato and M. Gatto, *Philos. Mag. B*,1993, **68**, 215.

Table of content entry

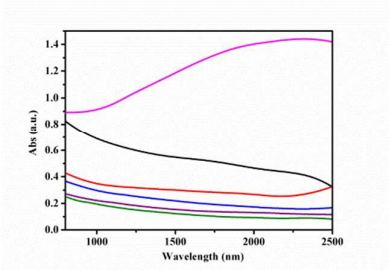

Aluminum-doped ZnO nanoparticles with tunable NIR absorption